

Tunable quantum criticality in multi-component Rydberg arrays

Natalia Chepiga¹

¹*Kavli Institute of Nanoscience, Delft University of Technology, Lorentzweg 1, 2628 CJ Delft, The Netherlands*

(Dated: August 25, 2023)

Arrays of Rydberg atoms have appeared as a remarkably rich playground to study quantum phase transitions in one dimension. One of the biggest puzzles that was brought forward in this context is a commensurate-incommensurate phase transitions out of density waves. Experiments report the transitions with dynamical critical exponent $z > 1$ that recent theoretical and numerical analysis attribute to the appearance of chiral transitions introduced by Huse and Fisher. However, further experimental exploration of these exotic transitions is complicated by the narrow parameter window where chiral transition can be realized. We argue that multi-component Rydberg arrays offer extra experimentally controllable parameters and provide a mechanism to tune quantum critical properties of the conformal Ashkin-Teller point that in turns controls the extent of the chiral transition. Here we consider an effective blockade model of two component Rydberg atoms - weak and strong components obeying nearest- and next-nearest-neighbor blockades. When laser detuning is applied to either strong or weak components the system is in the period-3 or period-2 phases correspondingly. However, laser detuning used for both components simultaneously stabilizes the period-4 phase partly surrounded by the chiral transition. We show that the extent of the chiral transition and even its appearance can be controlled by the relative ratio of the Rabi frequencies of the two components.

INTRODUCTION

Understanding the nature of quantum phase transitions in low-dimensional systems is one of the most exciting and challenging topics in condensed matter physics[1, 2]. Over the past decades numerous fascinating critical phenomena have been predicted in 1+1D by developments in conformal field theory[3, 4] and advances in numerical approaches such as the density matrix renormalization group algorithm (DMRG)[5–8]. Quantum simulators based on neutral Rydberg atoms trapped with optical tweezers have emerged as an amazing platform to further explore quantum critical phenomena in many-body systems[9, 10].

One of the most debated and long-standing problem in the theory of phase transitions is a chiral melting of the density-wave order the history of which roots back to the study of thermal melting of periodic phases in adsorbed monolayers[11–17]. Recent experiments on Rydberg atoms attracts new attention to this problem now in the context of one-dimensional (1D) quantum chains[10, 18–25]. The quantum many-body Hamiltonian of an array of Rydberg atoms can be formulated in terms of hard-core bosons:

$$H_{\text{Ryd}} = \sum_i \left[-\Omega(d_i^\dagger + d_i) - \Delta n_i + \sum_{R=1}^{+\infty} V_R n_i n_{i+R} \right] \quad (1)$$

where Ω is a Rabi frequency and $V_R = V \left(\frac{1}{R}\right)^6$ is the van der Waals potential. A competition between the laser detuning Δ that favors atoms to be in excited states and strong van der Waals interaction that blocks simultaneous excitation of multiple atoms within a certain radius leads to a sequence of density-wave lobes with integer periodicities[10, 25]. Since interaction between

Rydberg atoms depends on a distance, the energy cost associated with the domain wall bringing excited atoms closer is different from the energy cost of a domain wall that pushes Rydberg atoms further apart. As a result, a certain domain sequence (e.g. A|B|C|A) will always be energetically favored over the others (e.g. A|C|B|A) creating chiral perturbations that might have a drastic effect on quantum phase transitions out of period- p phases[15, 17, 26].

For $p = 2$ there are only two types of domains and no chiral perturbation arises (A|B|A vs B|A|B), thus the transition, if continuous, belongs to the Ising universality class. For $p \geq 5$ the transition takes place via an incommensurate Luttinger liquid phase (also known as a floating phase)[25]. The transition out of $p = 3$ is more complicated. Inside the disordered phase there is a commensurate line with the wave-vector $q = 2\pi/3$. Along this line chiral perturbations vanish and when it hits the boundary of the period-3 phase the transition is direct in the three-state Potts universality class. Away from this point chiral perturbations re-appear. They are relevant so the transition, if direct, is believed to be in the Huse-Fisher chiral universality[17, 19–21, 24]. Eventually this direct chiral transition turns into a two-step melting through an intermediate floating phase[19, 20, 25].

The most intriguing case is $p = 4$. Along the commensurate line with $q = \pi/2$, just as for $p = 3$ case, chiral perturbations vanish and the transition is conformal[22]. But for $p = 4$ the underlying critical theory is Ashkin-Teller that forms a *weak* universality class[4]. This implies that critical exponents, for instance ν that controls the divergence of the correlation length, can be continuously tuned by external parameters. Traditionally one use the Ashkin-Teller model (see e.g. Ref.[27]) that interpolates between two decoupled Ising chains at

$\lambda = 0$ and the four-state Potts point at $\lambda = 1$. The exponent ν as a function of λ is known exactly and given by $\nu = \frac{1}{2 - \frac{2}{\pi} [\arccos(-\lambda)]^{-1}}$ [27, 28]. Away from the commensurate line the system is incommensurate and chiral perturbations are present. But, as sketched in Fig.1, the appearance of a chiral transition depends on the properties of the Ashkin-Teller point along the commensurate line [11, 17, 29, 30]. When $\nu \gtrsim 0.8$ (this corresponds to $\lambda \lesssim 0.5$) the floating phase opens immediately; when $0.8 \lesssim \nu \leq (1 + \sqrt{3})/4 \approx 0.683$ (or $0.5 \lesssim \lambda \lesssim 0.978$) chiral perturbations are still relevant but for a while the transition remains direct in the chiral universality class followed by the floating phase that appears when chiral perturbations are strong [29, 30]; finally, when $0.683 \lesssim \nu \leq 2/3$ chiral perturbations are irrelevant and one can expect a finite (though perhaps small) interval of conformal transitions in the Ashkin-Teller universality class followed first by the direct chiral transition and then by the floating phase [30, 31]. It turns out that in the simplest array of Rydberg atoms the Ashkin-Teller point is characterized by the critical exponent $\nu \approx 0.78$ and the second scenario is realized. However, as illustrated in Fig.1, the closer the Ashkin-Teller commensurate point to $\lambda \approx 0.5$ (and $\nu \approx 0.8$) the shorter is the interval of the chiral transition. As a consequence, the chiral transition in the ordinary Rydberg array appears only over a very short interval in the vicinity of the conformal point [20]. For this reason the experimental investigation of this transition is a subject to a full control over parameters and noise and a high accuracy of experimental observations.

In this paper we investigate the possibility to manipulate an appearance and an extent of a chiral transition by tuning the properties of the Ashkin-Teller point. Full description of the chiral Ashkin-Teller model as sketched in Fig.1 requires three dimensional parameter space, however the model of Rydberg atoms introduced in Eq.1 has only two independent parameters - Δ/Ω and V/Ω . In recent years there were several proposals for Rydberg atoms aiming to add more experimentally controllable knobs. Among them the multi-species [32, 33] and multi-component [34, 35] Rydberg arrays seems the most promising. In multi-species setup the atoms of two (or, in principle, more) different sorts are used; often this corresponds to a certain arrangements of Cs and Rb atoms. In experiments the Rabi frequency, laser detuning and van der Waals potential can be individually controlled for each individual specimen in addition to the inter-species interaction. The effective model is defined by the six-dimensional parameter space. In multi-component Rydberg atoms, only one type of atoms is used (Rb or Cs) but each atom can be excited to one of the two Rydberg levels called components. These levels can be selected such that (i) interaction between two atoms excited to the first level are much weaker than the interaction between the atoms excited to the second level; and (ii) all other inter-

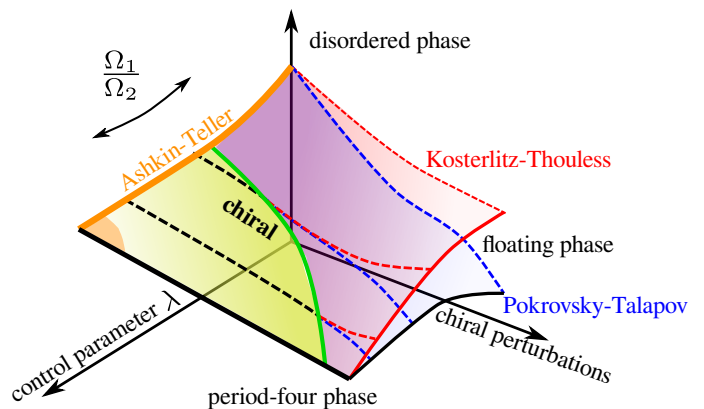


Figure 1. **Nature of the quantum phase transition between the period-four and disordered phases in the presence of chiral perturbations.** When there is no chiral perturbations the transition is conformal in the Ashkin-Teller universality class (orange line). Along this line the critical exponent ν is controlled by the parameter λ . When $0 \leq \lambda \lesssim 0.5$ (equivalently when $0.8 \lesssim \nu \leq 1$) the transition is a two step melting via Kosterlitz-Thouless (red) and Pokrovsky-Talapov (blue) transitions with an intermediate floating phase. When $0.5 \lesssim \lambda \lesssim 0.978$ ($0.683 \lesssim \nu \lesssim 0.8$) for small chiral perturbations the transition is direct and chiral (yellow). Green line states for the Lifshitz line separating the chiral transition from the floating phase. For $0.987 \lesssim \lambda \leq 1$ ($2/3 \leq \nu \lesssim 0.683$) small chiral perturbations are irrelevant and the transition remains conformal (orange area).

actions including those between atoms at different levels are negligibly small. The corresponding model has five independent parameters: inter-atomic spacing (that for a given pair of Rydberg levels defines the strength of the van der Waals potential for both components), two Rabi frequencies Ω_1 and Ω_2 and two individually controlled laser detunings Δ_1 and Δ_2 as sketched in Fig.2. Between two set-ups - multi-species and multi-component arrays - the latter has one significant advantage in the context of quantum phase transition and chiral melting: it preserves translation symmetry.

We study a ground-state phase diagram of the blockade model (see below) of the two-component Rydberg array. We show that: (i) when laser detunings are large for both components, the system is in the period-four phase with every other site occupied by the weak component and every fourth site occupied by the strong one; (ii) ratio between Rabi frequencies of the two components tunes the properties of the Ashkin-Teller multicritical point; (iii) by increasing Ω_1/Ω_2 one can extend the interval over which the chiral transition is realized, by decreasing this ratio one make chiral transition to disappear.

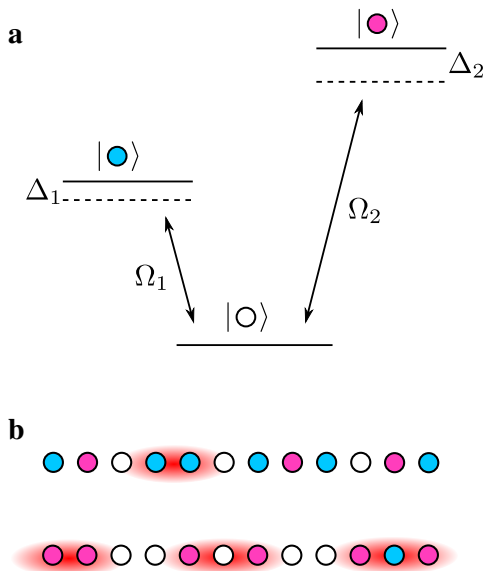


Figure 2. Sketch of the two-component Rydberg atom. (a) Atoms are excited to the two Rydberg levels $\alpha = 1, 2$ from the ground state by a laser with Rabi frequency Ω_α and detuning Δ_α . (b) Interaction at the first (second) level is weak (strong) and result in a nearest- (next-nearest-) neighbor blockade. Configurations that violate these blockades are marked with red ellipses. Note that we neglect inter-species interactions, thus two atoms excited to two different levels can be nearest-neighbors.

RESULTS

The blockade model

Because of the very fast increase of the van der Waals potential at short distances simultaneous occupation of atoms within certain blockade radius is essentially excluded. It allows us to approximate long-range interactions of two components with two types of Rydberg blockade: nearest-neighbor blockade for the weak component, and next-nearest-neighbor one for the strong one. The resulting model is defined by the following microscopic Hamiltonian:

$$H_{MC} = \sum_{\alpha=1,2} \sum_i \left[-\Omega_\alpha (d_{\alpha,i}^\dagger + d_{\alpha,i}) - \Delta_\alpha n_{\alpha,i} \right] \quad (2)$$

acting in a constrained Hilbert space:

$$n_{1,i} n_{1,i+1} = 0 \quad (3)$$

$$n_{2,i} n_{2,i+1} = n_{2,i} n_{2,i+2} = 0 \quad (4)$$

Here $d_{\alpha,i}^\dagger$ brings an atom at site i from the ground-state to the first (second) Rydberg level if $\alpha = 1$ ($\alpha = 2$). This model has three independent parameters that we define as Δ_1/Ω_1 , Δ_2/Ω_2 , and Ω_2/Ω_1 . We study the model with state-of-the-art DMRG algorithm[5–8] (see "Methods" for details of the algorithm).

Overview of the phase diagram

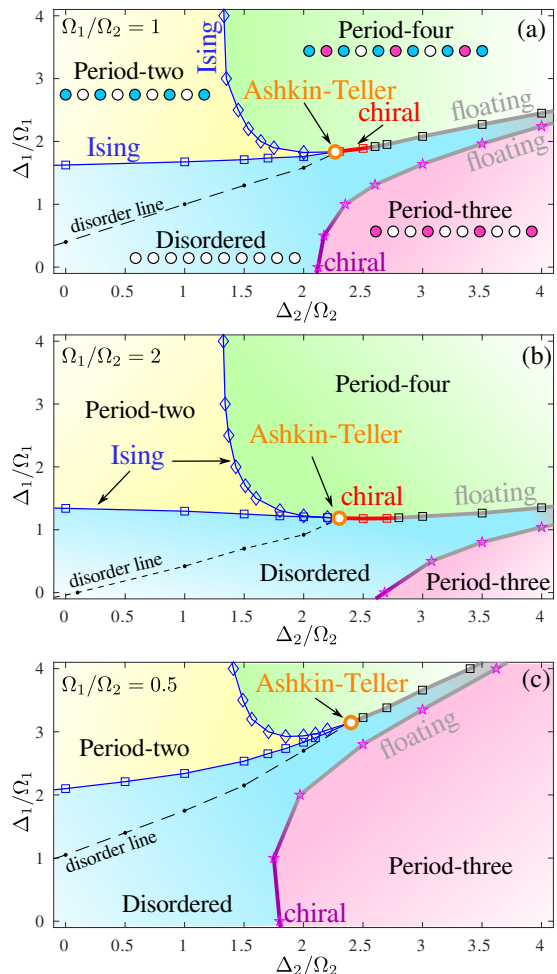


Figure 3. Phase diagrams of the blockade models defined by Eq.2 as a function of laser detuning of two species and for three relative ratio of Rabi frequencies Ω_1/Ω_2 . Each phase diagram contains four gapped phases: disordered phase, and three density wave-phases with periodicity $p = 2, 3$ and 4 . Typical patterns of these phases are sketched in (a) where white circles denote atoms in the ground state, blue and red circles state for atoms excited to the first (weak) and second (strong) Rydberg levels correspondingly. The period-2 phase is separated from the disordered and period-4 phases by two Ising transitions (blue squares and diamonds). The multicritical point (open orange circle) belongs to the Ashkin-Teller universality class. For some interval in (a) and (b) the transition to the period-4 phase is direct and chiral (red line). The key observation is that the extent of the chiral transition in (b) for $\Omega_1/\Omega_2 = 2$ is significantly larger than in (a) for $\Omega_1/\Omega_2 = 1$, while for $\Omega_1/\Omega_2 = 0.5$ in (c) the floating phase (gray) opens immediately. The transition between period-three phase and the disordered phase is chiral (purple line) for small values of Δ_1/Ω_1 and through a floating phase (gray) for large detuning of the weak component (see "Methods" for details).

We study the phase diagram as a function of Δ_1/Ω_1

and Δ_2/Ω_2 for three fixed values of the ratio of the Rabi frequencies $\Omega_2/\Omega_1 = 1, 2$ and $1/2$. The results are summarized in the phase diagrams in Fig.3. When laser detunings are small $\Delta_1, \Delta_2 \ll 1$ the system is in the disordered phase that does not break translation symmetry. For large Δ_2 and small Δ_1 the system is populated with the second (strong) component that due to the next-nearest-neighbor Rydberg blockade leads to a period-three density-wave phase. In the opposite limit of small Δ_2 and large Δ_1 the system is in the period-two phase with every other site occupied by a weak component with nearest-neighbor blockade. Upon increasing the detuning Δ_2 the translation symmetry is once again spontaneously broken and every other empty site that is not occupied by the weak component is now occupied by the strong one realizing a period-four phase as sketched in Fig.3(a).

From now on we are going to focus on the transitions out of period-four phase. One way to go from the disordered to the period-four phases is via the period-two phase. Along such a path the translation symmetry is first spontaneously broken by two sites at the disordered to period-two transition that belongs to the Ising universality class (see "Methods"). Then, for each of the two ground-states the translation symmetry is broken once again by two and the system undergoes the second Ising transition into the period-four phase. For larger values of Δ_2/Ω_2 the two Ising critical lines come closer and eventually merge into a multicritical point in the Ashkin-Teller universality class. Beyond this point the transition from the disordered to the period-four phases is either direct in the chiral universality class or via the floating phase as shown in Fig.3. This is consistent with the observation that the disorder line (see "Methods") at which the weak component develops incommensurability goes into the multicritical point. Strong component seems to be always incommensurate in the disordered phase however inside the period-two phase we see a crossover between commensurate and incommensurate regimes.

Extent of the chiral transition

In order to distinguish three types of transitions - Ashkin-Teller, chiral and floating phase - we look at the product $|q - \pi/2| \times \xi$, where q is incommensurate wave-vector approaching its commensurate value with the critical exponent $\bar{\beta}$ and ξ is a correlation length diverging at the transition the critical exponent ν . To the best of our knowledge for the Ashkin-Teller critical theory the exact value of $\bar{\beta}$ is not known, but Huse and Fisher argued that for conformal transition $\bar{\beta} > \nu$ [15, 17]. This implies that upon approaching the Ashkin-Teller point the product $|q - \pi/2| \times \xi$ vanishes. By contrast, at the chiral transition, though exact values of the exponents $\bar{\beta}$ and ν are not known, the equality $\nu = \bar{\beta}$ should hold thus the prod-

uct $|q - \pi/2| \times \xi$ takes some finite value. When intermediate floating phase emerges, it is separated from the disordered phase by the Kosterlitz-Thouless transition[36]. Upon approaching this transition the correlation length diverges stretch-exponentially, while the wave-vector q remains incommensurate across the transition. Therefore the product $|q - \pi/2| \times \xi$ is expected to diverge.

In addition, we also look at the critical exponent ν' that controls the divergence of the correlation length in the ordered phase. When transition is direct the correlation length diverges symmetrically on both sides of the critical line and the two exponents are equal $\nu = \nu'$. For the Ashkin-Teller transition it is in the range $2/3 \leq \nu, \nu' \leq 1$. In case of the floating phase the transition to the period-four phase belongs to the Pokrovsky-Talapov universality class[37] characterized by the critical exponent $\nu' = 1/2$.

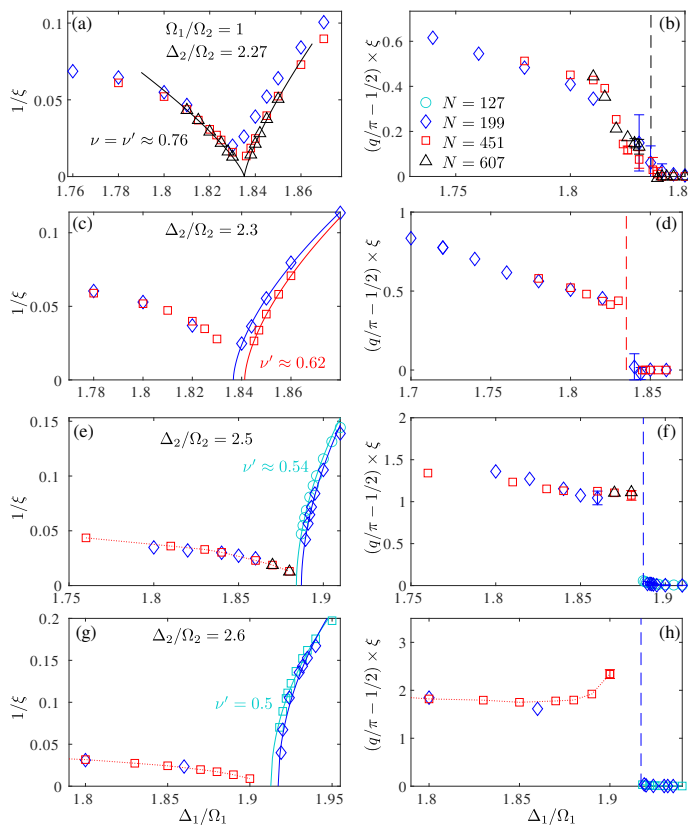


Figure 4. **Inverse of the correlation length and the product $|q - \pi/2| \times \xi$ along four cuts across the transition for $\Omega_1/\Omega_2 = 1$.** (a),(b) - a vertical cut through an Ashkin-Teller point at $\Delta_1/\Omega_2 = 2.27$; (c)-(f) two cuts through a chiral transition; (g),(h) - a cut through a floating phase. In (a) correlation lengths are fitted with the power law with equal critical exponents $\nu = \nu'$. $|q - \pi/2| \times \xi$ is defined with errorbars $2 \times \xi^2/N^2$, we only show errorbars if they exceed the size of the symbols. Dashed lines show the boundary of the ordered phase extracted by fitting the correlation length, color code corresponds to the one listed in (b).

In Fig.4 we show the inverse of the correlation length

and the product $|q - \pi/2| \times \xi$ across four different cuts through the transition for $\Omega_1/\Omega_2 = 1$. At $\Delta_2/\Omega_2 = 2.27$ as shown in Fig.4(a) the divergence of the correlation length is symmetric and numerically extracted critical exponent $\nu = \nu' \approx 0.76 \pm 0.02$ is consistent with the Ashkin-Teller critical theory. We also see in Fig.4(b) that the product $|q - \pi/2| \times \xi$ vanishes at this transition.

The identified Ashkin-Teller point is inside the interval $2/3 \leq \nu \lesssim 0.8$ where chiral transition has been predicted[29, 30]. Indeed, already at $\Delta_2/\Omega_2 = 2.3$ the product $|q - \pi/2| \times \xi$ takes some finite value signaling the appearance of the chiral transition as shown in Fig.4(d). This picture remains valid up to $\Delta_2/\Omega_2 = 2.5$, as shown in Fig.4(f). In order to locate the transition, we fit the correlation length with a power law with critical exponent ν' . For all cuts we see a finite-size effect in the location of the transition - it shifts towards the ordered phase. This effect is very common in Rydberg atoms[20]. For $\Delta_2/\Omega_2 = 2.6$ we see a sign of divergence of $|q - \pi/2| \times \xi$ as shown in Fig.4(h); furthermore the scaling of the correlation length is in excellent agreement with the Pokrovsky-Talapov critical exponent $\nu' = 1/2$. To summarize, for the ratio $\Omega_1/\Omega_2 = 1$ we detect the chiral transition to the period-four phase over the interval $2.27 < \Delta_2/\Omega_2 \lesssim 2.55$ and we identified the Ashkin-Teller multicritical point compatible with this scenario.

For the larger ratio of Rabi frequencies $\Omega_1/\Omega_2 = 2$ the Ashkin-Teller point is located at $\Delta_2/\Omega_2 \approx 2.3$ and is characterized by the critical exponent $\nu \approx 0.68 \pm 0.04$ as presented in Fig.5(a),(b). Beyond this point we detect the chiral transition that extends at least up to $\Delta_2/\Omega_2 = 2.7$ (see Fig.5(c),(d)). At $\Delta_2/\Omega_2 = 2.8$ we see a clear signature of the floating phase Fig.5(e),(f). The larger interval of the chiral transition compare to $\Omega_1/\Omega_2 = 1$ is fully consistent with smaller critical exponent ν at the Ashkin-Teller point. In other words, by increasing Ω_1/Ω_2 we tune the multicritical Ashkin-Teller point towards larger λ and smaller ν , that in turns lead to a longer chiral transition as sketched in Fig.1. Note also that the difference between the chiral transition and floating phase is more pronounced for $\Omega_1/\Omega_2 = 2$, for comparison see Fig.5(c)-(f) and Fig.4(e)-(h). Thus, larger Ω_1/Ω_2 can provide a by-path to locate the Lifshitz point where chiral transition turns into a floating phase and to study its properties.

Now let us see how the picture changes when the ratio of Rabi frequencies decreases to $\Omega_1/\Omega_2 = 0.5$. In this case, the multicritical point is located very close to the floating phase at the boundary of the period-three phase. As a result, correlation lengths are very large all over the narrow window of the disordered phase. This prevents us from fitting the correlation length inside the disordered phase but the product $|q - \pi/2| \times \xi$ computed locally remains a valid measure. As shown in Fig.6(b) $|q - \pi/2| \times \xi$ goes to zero at $\Delta_2/\Omega_2 = 2.4$ which we then associate with the Ashkin-Teller point, while for $\Delta_2/\Omega_2 = 2.5$ pre-

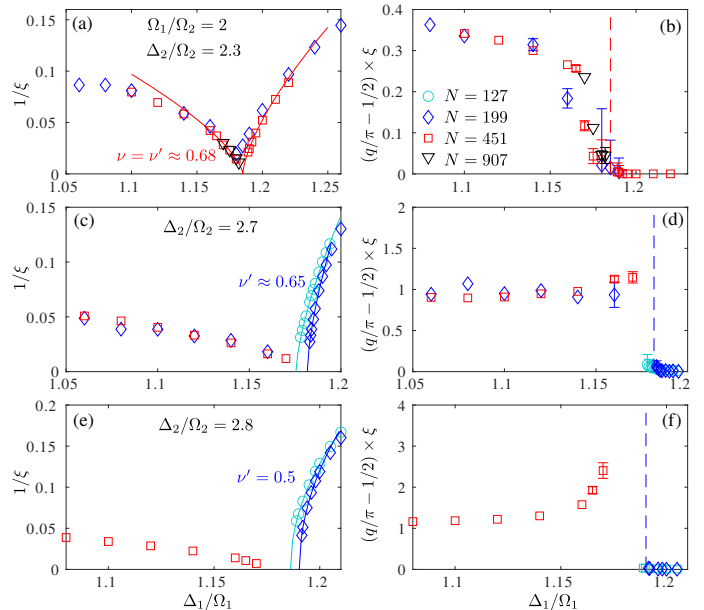


Figure 5. Inverse of the correlation length and the product $|q - \pi/2| \times \xi$ along three cuts across the transition for $\Omega_1/\Omega_2 = 2$. (a),(b) - a vertical cut through an Ashkin-Teller point at $\Delta_1/\Omega_2 = 2.3$; (c),(d) a cut through a chiral transition at $\Delta_1/\Omega_2 = 2.7$; (e),(f) - a cut through a floating phase. In (a) correlation lengths are fitted with the power law with equal critical exponents $\nu = \nu'$. $|q - \pi/2| \times \xi$ is defined with errorbars $2 \times \xi^2/N^2$, we only show errorbars if they exceed the size of the symbols. Dashed lines show the boundary of the ordered phase extracted by fitting the correlation length for systems, color code corresponds to the one listed in (b).

sented in Fig.6(d) it already shows a signature of divergence signaling the presence of the floating phase. The latter is further supported our results for the correlation length in Fig.6(c) that are in excellent agreement with the Pokrovsky-Talapov transition. The picture is completed by the observation that upon approaching the Ashkin-Teller point along $\Delta_2/\Omega_2 = 2.4$ the correlation length diverges with the critical exponent $\nu' \approx 0.81$ - outside of the interval $2/3 \leq \nu \lesssim 0.8$ where chiral transition is possible. Of course, neither this interval nor the critical exponents ν' are exact and we cannot exclude a possibility of a short chiral transition between $\Delta_2/\Omega_2 = 2.4$ and 2.5. But what we observe here is a very important tendency that the Ashkin-Teller critical exponent increases and the chiral transition becomes significantly shorter to the point when it actually disappears.

DISCUSSION

Our results offer a novel approach to manipulate quantum criticality in Rydberg atoms experiments. Currently the main bottleneck for systematic investigation of chiral

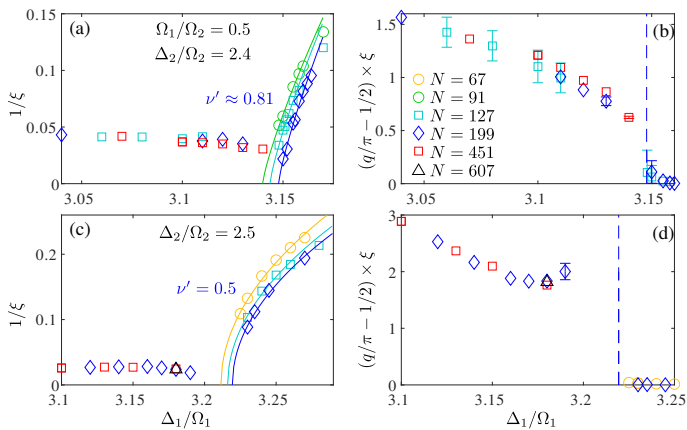


Figure 6. **Inverse of the correlation length and the product $|q - \pi/2| \times \xi$ along three cuts across the transition for $\Omega_1/\Omega_2 = 2$.** (a),(b) - a cut through an Ashkin-Teller point at $\Delta_1/\Omega_2 = 2.3$; (c),(d) a cut through a chiral transition at $\Delta_1/\Omega_2 = 2.7$; (e),(f) - a cut through a floating phase. In (a) correlation lengths are fitted with the power law with equal critical exponents $\nu = \nu'$. $|q - \pi/2| \times \xi$ is defined with errorbars $2 \times \xi^2/N^2$, when errorbars are not shown they do not exceed the size of the symbols. Dashed blue lines show the boundary of the ordered phase extracted by fitting the correlation length for systems with $N = 199$.

transitions out of period-four phase in Rydberg arrays is an extremely small interval in the parameter space where this chiral transition is realized. Our findings open a way to control an extent of this exotic quantum phase transition granting access to multiple well separated and distinguishable paths across it. This is necessary to identify universal and non-universal properties of the chiral transition and to formalize the definition of the $p = 4$ chiral universality class.

Furthermore, our observations creates an opportunity to verify all theoretically predicted regimes of the chiral Ashkin-Teller model obtained with extensive numerical simulations with corner transfer matrix renormalization group (CTMRG)[29] and DMRG algorithms[30] that were summarized in Fig.1. But to the best of our knowledge neither classical nor quantum version of this phase diagram has been probed experimentally.

In the present paper we have studied the simplest two component arrangements. Generalization to three and more components is conceptually straightforward and introduces a new class of models with multi-component Hilbert space. In experiments each component requires its own set of lasers so practically the number of components will be limited to just a few. But multiple individually controllable parameters also enables a possibility of fine-tuning, for instance to the point with higher emergent symmetries etc.

We expect our results obtained for the blockade approximation to be qualitatively correct for the model

with $1/r^6$ potential as soon as the selected Rydberg levels and the lattice spacing are such that detuning of weak and strong components alone leads to stable period-two and period-three phases correspondingly. It would be interesting to explore models with different interaction regimes, for instance, with longer blockades. It worth to mention that multi-component Rydberg arrays offer a unique opportunity to study fusion properties of chiral transitions. Let us imagine a situation when the weak component obeys the next-nearest-neighbor blockade and leads to a period-three phase bounded, at least partially, by the chiral transition. What would be the nature of the multicritical point if instead of two Ising transitions in Fig.3 one of them or even two will be chiral? We leave this question open for future experimental and theoretical investigations.

METHODS

Details about the algorithm

We perform numerical simulations with DMRG algorithm in the form of variational optimization of the matrix product states (MPS)[5–8]. We implement the blockade by applying a strong penalty terms $U(n_{1,i}n_{1,i+1} + n_{2,i}n_{2,i+1} + n_{2,i}n_{2,i+2})$. We choose the penalty to be $U = 400$: this value is sufficiently strong to keep expectation value of any of the three terms listed above below 10^{-6} even in the vicinity of the transition, while this value is not too large to cause instabilities and convergence issues. We also benchmarked our algorithm with constrained DMRG with explicitly implemented blockades: the two sets of results do not have any noticeable differences. Quite surprisingly the unconstrained DMRG with the penalty terms turns out to be more efficient for numerical simulations of multi-component Rydberg arrays than the constrained version of the algorithm that by construction obeys a block-diagonal structure. Contracting the networks block-by-block allows to reduce the memory cost significantly, however in the present case an auxiliary bond of tensors has seven different labels leading to a large number of rather small blocks such that an over-head for a block-by-block operation turns out to be higher than the gain from the lower memory cost. In DMRG simulations we reach the convergence of the systems with up to $N = 907$ sites keeping up to 2500 states and performing up to 8 sweeps; we generically discard singular values below 10^{-8} .

Location of the Ising transitions

In order to locate Ising transitions we look at the finite-size scaling of the density oscillations - a local measure of spontaneously broken translation symmetry. In the

period-two phase the translation symmetry is broken by the weak component and by two sites, so the relevant operator is defined as $D_1 = |\langle n_{1,j} \rangle - \langle n_{1,j+1} \rangle|$ that we compute in the middle of the chain. We look at this quantity in the log-scale and associate the transition with the separatrix that separates disordered phase (concave curves) and the symmetry broken phase (convex ones) as shown in Fig.10(a). The slope of the separatrix corresponds to the scaling dimension that is in excellent agreement with the conformal field theory prediction for the Ising transition $d_I = 1/8$ [4].

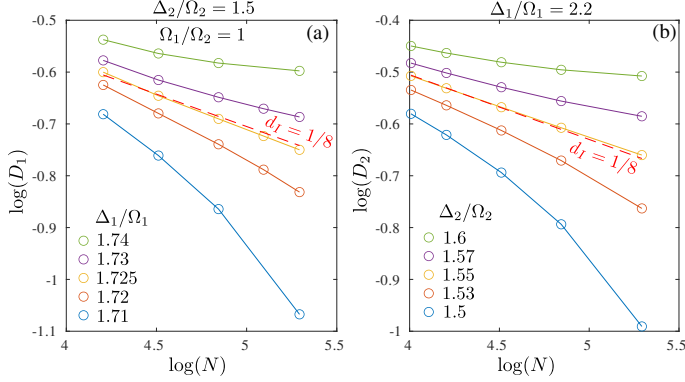


Figure 7. **Finite-size scaling of the local density oscillations across two Ising transitions.** Scaling of the local density oscillations in (a) weak component across the transition between the disordered and period-two phases and (b) in strong component across the transition between the period-two and period-four phases. In each case the separatrix is associated with the transition and the slope agree with the Ising scaling dimension $d = 1/8$ (dashed red line) shown for a reference.

At the transition to the period-four phase the translation is again spontaneously broken: every other site that was not occupied by the weak component in the period-two phase becomes occupied by the strong component in the period-four phase. So the local order parameter can be defined as $D_2 = |\langle n_{2,j} \rangle - \langle n_{2,j+2} \rangle|$, where $j, j+2$ are sites that are not occupied by the weak component. As previously, we associate the transition with the separatrix and its slope is in excellent agreement with the Ising scaling dimension $1/8$ (see Fig.10(b)).

Extraction of the correlation length and of the wave-vector

In order to extract the correlation length and the wave-vector q , we fit the connected correlation function for the strong component $C_{i,j} = \langle n_{2,i} n_{2,j} \rangle - \langle n_{2,i} \rangle \langle n_{2,j} \rangle$ to the Ornstein-Zernicke form[38]:

$$C_{i,j}^{\text{OZ}} \propto \frac{e^{-|i-j|/\xi}}{\sqrt{|i-j|}} \cos(q|i-j| + \varphi_0), \quad (5)$$

where the correlation length ξ , the wave vector q , and the initial phase φ_0 are fitting parameters. We extract the correlation length and the wave-vector in two steps. First, we discard the oscillations and fit the main slope of the decay as shown in Fig.8(a) such that the fit can be performed in a semi-log scale $\log C(x = |i-j|) \approx c - x/\xi - \log(x)/2$. This provides more accurate estimates of the correlation length on a long scale. Second we fit the reduced correlation function

$$\tilde{C}_{i,j} = C_{i,j} \frac{\sqrt{|i-j|}}{e^{-|i-j|/\xi+c}} \quad (6)$$

with a cosine $\tilde{C}_{i,j} \approx a \cos(q|i-j| + \varphi_0)$ as shown in Fig.8(b). The agreement between the DMRG data (blue dots) and the fit (red circles) is almost perfect. We estimate error in q caused by finite-size effects as $2\pi\xi/N^2$, where $2\pi/N$ is a natural step in q due to fixed boundary conditions and assuming for infinite correlation length, an additional factor ξ/N reflect the possibility to adjust q at the edges when correlation length is finite.

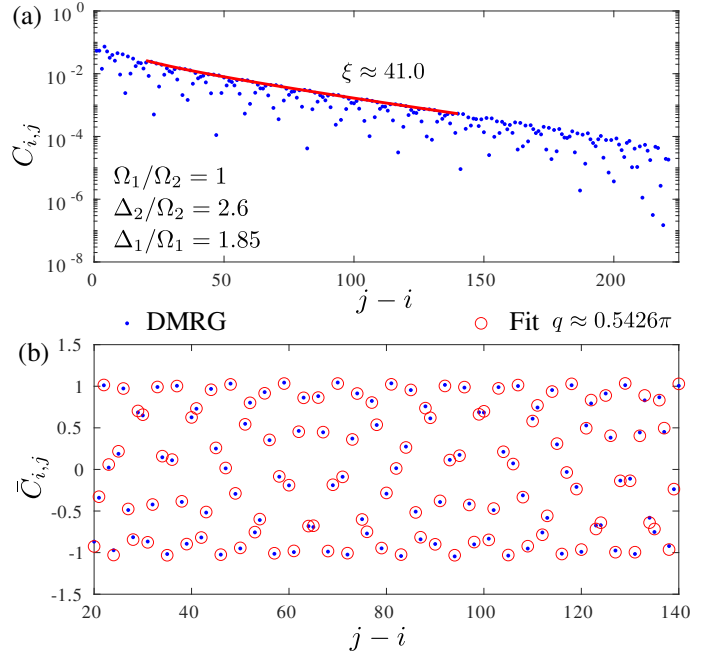


Figure 8. **Example of fit of the correlation function to the Ornstein-Zernicke form.** In the first step (a), we extract the correlation length discarding the oscillations. In the second step (b), we fit the reduced correlation function and extract the wave-vector q .

Transition out of period-three phase

In order to locate the boundary of the period-three phase and to identify the nature of the transition we follow a similar procedure as for the boundary of the period-four phase. We look at the product $|2\pi/3 - q| \times \xi$ that

is expected to take a finite value if transition is chiral and diverge in the case of intermediate floating phase. Here we expect conformal Potts point only in the limit $\Delta_1/\Omega_1 \rightarrow \infty$. We also look at the scaling of the correlation length in the period-three phase. In Fig.9 we provide an example of two typical cuts through the transition for $\Omega_1/\Omega_2 = 1$: when it is chiral in Huse-Fisher universality class in Fig.9(a),(b); and when it goes through an intermediate floating phase in Fig.9(c),(d).

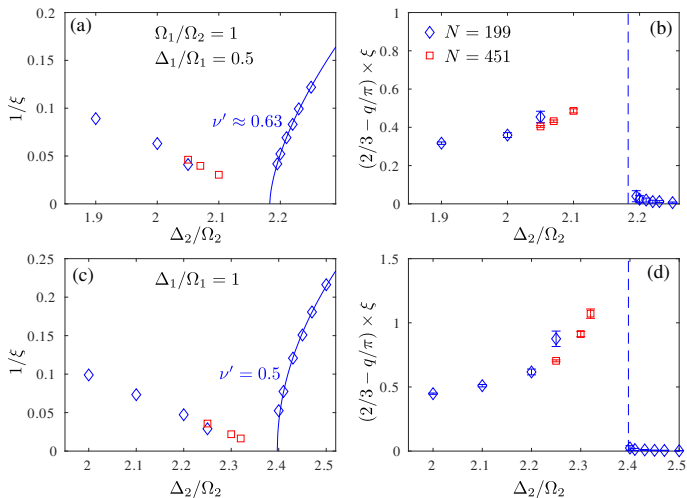


Figure 9. **Inverse of the correlation length and the product $|2\pi/3 - q| \times \xi$ along two horizontal cuts across the transition to the period-three phase for $\Omega_1/\Omega_2 = 1$.** (a),(b) - a cut through a chiral transition point at $\Delta_1/\Omega_1 = 0.5$; (c),(d) a cut through the floating phase at $\Delta_1/\Omega_1 = 1$. In (a) and (c) the correlation lengths in the period-three phase are fitted with the power law. Dashed blue lines show the boundary of the ordered phase extracted in (a) and (c).

Following the same procedure we identified the boundaries of the period-three phase for $\Omega_1/\Omega_2 = 2$ and 0.5 . For $\Omega_1/\Omega_2 = 2$ our results at $\Delta_1/\Omega_1 = 0$ are consistent with chiral transition, while already at $\Delta_1/\Omega_1 = 0.5$ we see a presence of the floating phase. For $\Omega_1/\Omega_2 = 0.5$ chiral transition is stable up to $\Delta_1/\Omega_1 = 1$ and the floating phase is detected at $\Delta_1/\Omega_1 = 2$.

Disorder line

Chiral perturbations usually manifest itself in incommensurate correlations. The line where real-space correlations switch from commensurate to incommensurate regimes is usually called in the literature the disorder line. In order to locate this line in the disordered phase we look at the connected correlations of the weak component. A few examples of commensurate and incommensurate scalings are shown in Fig.10; we associate the disorder line with the point where incommensurability disappears. Calculations were performed with $N = 67$

sites deep inside the disordered phase and with $N = 91$ in the vicinity of the multicritical point.

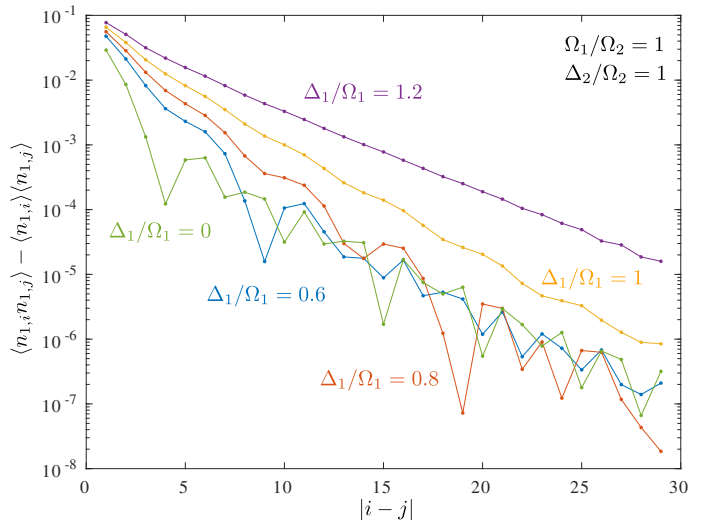


Figure 10. **Location of the disorder line.** Scaling of the weak component correlations as a function of distance for $\Omega_1/\Omega_2 = 1$ and $\Delta_2/\Omega_2 = 1$. For $\Delta_1/\Omega_1 < 1$ one can clearly see the presence of incommensurability that disappears for $\Delta_1/\Omega_1 > 1$.

It is not always clear whether the system is commensurate or incommensurate (see for instance the yellow line in Fig.10) and for this reason there is an uncertainty in the location of disorder line. However, our results are consistent with the disorder line hitting the period-four phase at multi-critical point. This agrees with expectation that system is commensurate on both sides of the Ising transition. In fact the situation is more subtle here. There are two components and two commensurate Ising transitions. At the transition between the disordered and the period-two phase the weak component breaks translation symmetry and this particular component has to be commensurate in the vicinity of the transition, however the strong component can remain incommensurate across this Ising transition. But at the second Ising transition from period-two to period four phases it is now the strong component that breaks the translation symmetry and thus it has to be commensurate in the vicinity of the transition. It implies that in principle there must be a second disorder line where incommensurability develops in the strong component; this line can be located in the period-two or in the disordered phase and also expected to end at the multicritical Ashkin-Teller point.

-
- [1] T. Giamarchi, *Quantum physics in one dimension*, Internat. Ser. Mono. Phys. (Clarendon Press, Oxford, 2004).
 - [2] A. M. Tsvelik, *Quantum Field Theory in Condensed Matter Physics*, 2nd ed. (Cambridge University Press, 2003).

- [3] J. Cardy, *Scaling and Renormalization in Statistical Physics*, Cambridge Lecture Notes in Physics (Cambridge University Press, 1996).
- [4] P. Di Francesco, P. Mathieu, and D. Sénéchal, *Conformal Field Theory*, Graduate Texts in Contemporary Physics (Springer, New York, 1997).
- [5] S. R. White, Phys. Rev. Lett. **69**, 2863 (1992).
- [6] U. Schollwöck, Rev. Mod. Phys. **77**, 259 (2005).
- [7] S. Östlund and S. Rommer, Phys. Rev. Lett. **75**, 3537 (1995).
- [8] U. Schollwöck, Annals of Physics **326**, 96 (2011).
- [9] H. Bernien, S. Schwartz, A. Keesling, H. Levine, A. Omran, H. Pichler, S. Choi, A. S. Zibrov, M. Endres, M. Greiner, V. Vuletić, and M. D. Lukin, Nature **551**, 579 (2017).
- [10] A. Keesling, A. Omran, H. Levine, H. Bernien, H. Pichler, S. Choi, R. Samajdar, S. Schwartz, P. Silvi, S. Sachdev, P. Zoller, M. Endres, M. Greiner, Vuletić, V. , and M. D. Lukin, Nature (London) **568**, 207 (2019).
- [11] M. den Nijs, Phase Transitions and Critical Phenomena **12**, 219 (1988).
- [12] J. Schreiner, K. Jacobi, and W. Selke, Phys. Rev. B **49**, 2706 (1994).
- [13] D. L. Abernathy, S. Song, K. I. Blum, R. J. Birgeneau, and S. G. J. Mochrie, Phys. Rev. B **49**, 2691 (1994).
- [14] W. Selke and J. M. Yeomans, Zeitschrift für Physik B Condensed Matter **46**, 311 (1982).
- [15] D. A. Huse and M. E. Fisher, Phys. Rev. Lett. **49**, 793 (1982).
- [16] D. A. Huse, A. M. Szpilka, and M. E. Fisher, Physica A: Statistical Mechanics and its Applications **121**, 363 (1983).
- [17] D. A. Huse and M. E. Fisher, Phys. Rev. B **29**, 239 (1984).
- [18] N. Chepiga and F. Mila, SciPost Phys. **6**, 33 (2019).
- [19] N. Chepiga and F. Mila, Phys. Rev. Lett. **122**, 017205 (2019).
- [20] I. A. Maceira, N. Chepiga, and F. Mila, Phys. Rev. Res. **4**, 043102 (2022).
- [21] G. Giudici, A. Angelone, G. Magnifico, Z. Zeng, G. Giudice, T. Mendes-Santos, and M. Dalmonte, Phys. Rev. B **99**, 094434 (2019).
- [22] N. Chepiga and F. Mila, Nature Communications **12**, 1 (2021).
- [23] S. Whitsitt, R. Samajdar, and S. Sachdev, Phys. Rev. B **98**, 205118 (2018).
- [24] R. Samajdar, S. Choi, H. Pichler, M. D. Lukin, and S. Sachdev, Phys. Rev. A **98**, 023614 (2018).
- [25] M. Rader and A. M. Läuchli, “Floating phases in one-dimensional rydberg ising chains,” (2019), arXiv:1908.02068 [cond-mat.quant-gas].
- [26] S. Ostlund, Phys. Rev. B **24**, 398 (1981).
- [27] M. Kohmoto, M. den Nijs, and L. P. Kadanoff, Phys. Rev. B **24**, 5229 (1981).
- [28] A. O’Brien, S. D. Bartlett, A. C. Doherty, and S. T. Flammia, Phys. Rev. E **92**, 042163 (2015).
- [29] S. Nyckees and F. Mila, Physical Review Research **4**, 013093 (2022).
- [30] B. Lüscher, F. Mila, and N. Chepiga, arXiv e-prints , arXiv:2308.07144 (2023), arXiv:2308.07144 [cond-mat.str-el].
- [31] H. J. Schulz, Phys. Rev. B **28**, 2746 (1983).
- [32] K. Singh, S. Anand, A. Pocklington, J. T. Kemp, and H. Bernien, Phys. Rev. X **12**, 011040 (2022).
- [33] C. Sheng, J. Hou, X. He, K. Wang, R. Guo, J. Zhuang, B. Mamat, P. Xu, M. Liu, J. Wang, and M. Zhan, Phys. Rev. Lett. **128**, 083202 (2022).
- [34] E. Levi, J. Minář, J. P. Garrahan, and I. Lesanovsky, New Journal of Physics **17**, 123017 (2015), arXiv:1503.03259 [physics.atom-ph].
- [35] Z. Lan, W. Li, and I. Lesanovsky, Phys. Rev. A **94**, 051603 (2016), arXiv:1605.01005 [cond-mat.quant-gas].
- [36] J. M. Kosterlitz and D. J. Thouless, Journal of Physics C: Solid State Physics **6**, 1181 (1973).
- [37] V. L. Pokrovsky and A. L. Talapov, Phys. Rev. Lett. **42**, 65 (1979).
- [38] L. Ornstein and F. Zernike, Koninklijke Nederlandse Akademie van Wetenschappen Proceedings Series B Physical Sciences **17**, 793 (1914).

ACKNOWLEDGMENTS

The author thanks Bernhard Lüscher, Samuel Nyckees and Frederic Mila for insightful discussions on the chiral Ashkin-Teller model and to Jiri Minar for inspiring discussion on multi-component Rydberg arrays. This work has been supported by the Delft Technology Fellowship and it was performed in part at Aspen Center for Physics, which is supported by National Science Foundation grant PHY-2210452. Numerical simulations have been performed at the DelftBlue HPC and at the Dutch national e-infrastructure with the support of the SURF Cooperative.